Water Research 163 (2019) 114852

Contents lists available at ScienceDirect

Water Research

journal homepage: www.elsevier.com/locate/watres

Assessing catchment scale flood resilience of urban areas using a grid cell based metric

Yuntao Wang [a, b], Fanlin Meng [b, *], Haixing Liu [a], Chi Zhang [a, **], Guangtao Fu [b]

[a] School of Hydraulic Engineering, Dalian University of Technology, Dalian, 116024, China
[b] Centre for Water Systems, College of Engineering, Mathematics and Physical Sciences, University of Exeter, North Park Road, Harrison Building, Exeter, EX4 4QF, UK

ARTICLE INFO

Article history:
Received 31 March 2019
Received in revised form
3 July 2019
Accepted 8 July 2019
Available online 10 July 2019

Keywords:
Grid cell
Flood resilience
Flood severity
System performance
Urban surface flooding

ABSTRACT

Urban flooding has become a global issue due to climate change, urbanization and limitation in the capacity of urban drainage infrastructures. To tackle the growing threats, it is crucial to understand urban surface flood resilience, i.e., how urban drainage catchments can resist against and recover from flooding. This study proposes a grid cell based resilience metric to assess urban surface flood resilience at the urban drainage catchment scale. The new metric is defined as the ratio of the number of unflooded grid cells to the total grid cell number in an urban drainage catchment. A two-dimensional Cellular Automata based model CADDIES is used to simulate urban surface flooding. This methodology is demonstrated using a case study in Dalian, China, which is divided into 31 urban drainage catchments for flood resilience analysis. Results show the high resolution resilience assessment identifies vulnerable catchments and helps develop effective adaptation strategies to enhance urban surface flood resilience. Comparison of the new metric with an existing metric reveals that new metric has the advantage of fully reflecting the changing process of system performance. Effectiveness of adaptation strategies for enhancing urban surface flood resilience is discussed for different catchments. This study provides a new way to characterize urban flood resilience and an in-depth understanding of flood resilience for urban drainage catchments of different characteristics, and thus help develop effective intervention strategies for sustainable sponge city development.

1. Introduction

Urban surface flooding, exacerbated by climate change and rapid urbanization, has caused grave negative consequences in many cities worldwide over the past decades (Hammond et al., 2015; Löwe et al., 2017; Wang et al., 2018). In the summer of 2007, 55,000 properties in the UK were flooded with an estimated economic loss of £3.2 billion (Pitt, 2008). The flood event in July 2012 in Beijing led to 79 deaths and an estimated economic loss of 11.64 billion yuan (£1.29 billion) (Yin et al., 2016). To tackle urban flooding, significant efforts have been made in developing flood assessment methods or frameworks (Hirabayashi et al., 2013; Jenkins et al., 2017; Morrison et al., 2017), which are essential to support decision-making for investment on flood management schemes such as the sponge city initiative in China (Jia et al., 2017). However, the current practice mainly focuses on the assessment of flood risk, i.e. the product of the likelihood of flooding and the related consequence. Greater efforts are required to assess system resilience, which is a concept firstly introduced in ecology (Holling, 1973) and has been applied in many engineering fields to measure the ability of a system to respond and recover from failures under exceptional conditions (Holling, 1996; Hu et al., 2018; Lee and Kim, 2017a, 2017b; Liao, 2012; Linkov et al., 2014; Meng et al., 2018; Mugume et al., 2015; Simonovic, 2016; Sweetapple et al., 2018). By incorporating resilience in urban flooding assessment and management, existing drainage capacity of an area can be better utilized and investment can be focused on places that are less resilient to flooding.

Indeed, there is a growing awareness to include resilience assessment in urban design and management. For example, the UK government urges resilience to be considered at all especially early stages of infrastructure works such as investment decisions and

* Corresponding author.
** Corresponding author.
E-mail addresses: M.Fanlin@exeter.ac.uk (F. Meng), czhang@dlut.edu.cn (C. Zhang).

https://doi.org/10.1016/j.watres.2019.114852

strategic planning (Gallego-Lopez and Essex, 2016). This has been enforced in industrial practice, e.g. water companies in England and Wales are required to incorporate resilience analysis in business plans on public water supply and sewer networks (Defra, 2016; Ofwat, 2017). However, no conceptual frameworks and evaluation standards were provided and no clear methodologies for resilience analysis were provided in the regulations or guidelines, which are essential for effective delivery of resilience.

Conceptual frameworks and metrics have been proposed in literature for the assessment and quantification of flood resilience (Batica, 2015; Bertilsson et al., 2019; Kotzee and Reyers, 2016; Lee and Kim, 2017b; Miguez and Veról, 2017; Restemeyer et al., 2015). Bruneau et al. (2003) developed a framework for assessing seismic resilience of communities, measured by robustness, rapidity, resourcefulness and redundancy in the technical, organizational, social and economic dimensions. Restemeyer et al. (2015) developed a heuristic framework for qualitative assessment of flood resilience cities, where resilience is defined by robustness, adaptability and transformability corresponding to various appraisal measures. Multi-criteria indices are commonly proposed for measuring the multifaceted flooding resilience (Bertilsson et al., 2019; Chen and Leandro, 2019; Kotzee and Reyers, 2016). For example, a spatialized urban flood resilience index (S-FRESI) was proposed to quantify resilience by flood risk and vulnerability, household's income and drainage capacities (Bertilsson et al., 2019). Chen and Leandro (2019) developed a Flood Resilience Index (FRI) that estimated performance at both the failure and recovery phases by physical, and economic and social indicators respectively. Principal components analysis was employed to derive a composite index by integrating flood-related social, ecological, infrastructural and economic indicators (Kotzee and Reyers, 2016). Although these metrics encompass various factors that contribute to flood resilience, they heavily rely on subjective expert judgements for the selection and weighting of composing indicators. To guide central, large-scale infrastructure schemes such as the sponge city initiative, objective assessment of existing drainage capacity and spatial flooding resilience over a landscape is necessary.

Performance-based metrics provide a new way of assessing urban flood resilience. Based on the definition of resilience by Butler et al. (2014), i.e. “the degree to which the system minimizes level of service failure magnitude and duration over its design life when subjected to exceptional conditions”, a metric was proposed by Mugume et al. (2015) to evaluate resilience of urban drainage systems. It measures the severity (a function of failure magnitude and duration) of flooding when subject to different levels of structural failure. Lee and Kim (2017b) developed a resilience index for urban drainage systems based on flood damages, which occurs only when flood depth reaches a certain point. However, the one-dimensional (1D) sewer flow model, i.e., Storm Water Management Model (SWMM), was employed for flood modelling and the calculation of the aforementioned resilience indices. As such, they cannot simulate urban flood resilience at high spatial and temporal resolutions, which is jointly influenced by many factors such as topography and land cover type in addition to the drainage network capacity. Yet, the detailed, dynamic and spatial flooding assessment is essential to support the planning and design of intervention strategies of flood management schemes.

The aim of this study is to propose a performance-based analytical framework for assessing flood resilience at urban drainage catchment scale. A new resilience metric is proposed that can measure the spatial variation in response to extreme rainfall storm events. The Cellular Automata Dual-DraInagE Simulation (CADDIES) model (Guidolin et al., 2016), which is a two-dimensional (2D) flood model, is used for efficient and detailed simulation of urban surface flooding (i.e. location and magnitude of flooding) (Chen et al., 2012; Guidolin et al., 2012; Wang et al., 2018). The proposed framework is applied to Siergou (Dalian, China) with 31 catchments to identify the vulnerable areas and provide guidance for building resilient and sustainable cities. Discussion is made on the effectiveness of adaptation strategies on enhancing urban surface flood resilience.

2. Methodology

A key flood resilience index reported in literature, which is used for comparison in this work, is reviewed in Section 2.1. The proposed urban surface flood metric is defined in Section 2.2. The modelling platform for the simulation of urban flood used in this study is described in the final sub-section.

2.1. Flood resilience

Resilience is commonly defined as the capacity of a system to resist, withstand, rapidly recover from and adapt more readily to exceptional conditions. The concept can be illustrated by the framework proposed by Juan-García et al. (2017), where stressors, properties, metrics and interventions are defined for engineering resilience. In the case of urban flood resilience, the main stressor is rainfall storm and resilience is calculated by the loss in system functionality and recovery time (Bocchini et al., 2013; Hwang et al., 2015; Mugume et al., 2015) under a range of scenarios. The performance curve for an urban system under a specified extreme rainfall event is shown in Fig. 1. The black dotted line represents the original performance level of service and the black solid line shows the actual system performance (P_t). The value of system performance varies from 0 (i.e. total loss of system performance) to 1 (i.e. no loss). The initial level of service is 1, which decreases from t_s following an extreme rainfall event, reaches the minimum value of p_f at t_{ps}, restores from t_{pe} and fully recovers to the full level of service at t_e.

Flood severity is an aggregated representation of the level of system damage during the entire process, as shown by the shaded area in Fig. 1 and calculated as follows:

$$Sev = \frac{1}{t_n}\int_0^{t_n}[1 - p(t)]dt \tag{1}$$

where Sev is flood severity, and t_n is the total simulation time.

Mugume et al. (2015) proposed a simplified metric Res_0 by

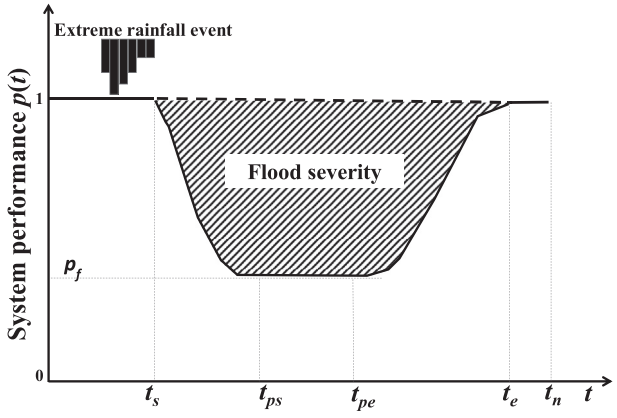

Fig. 1. System performance curve for an urban system under an extreme rainfall event.

approximating the flood severity *Sev* in Eq. (1) by a rectangular area as formulated in Eqs. (2) and (3).

$$Sev = \frac{V_{TF}}{V_{TI}} \times \frac{t_f}{t_n} \tag{2}$$

$$Res_0 = 1 - Sev = 1 - \frac{V_{TF}}{V_{TI}} \times \frac{t_f}{t_n} \tag{3}$$

where V_{TF} is the total flood volume, V_{TI} is total inflow into a drainage system, t_f is the mean duration of flooding across the entire network, and t_n is the total simulation time.

2.2. Flood resilience assessment

To measure resilience for complex networks, Ganin et al. (2016) assumed the nodes have only two possible states (i.e., active and inactive) and the percentage of nodes that are active are used to assess system performance. Following this idea, a new resilience metric, which is based on grid cells, is proposed in this study for the assessment of resilience at catchment levels. That is, a catchment is divided into grid cells, which have two possible states, i.e. flooded or unflooded, represented by the blue and white shaded cells in Fig. 2, respectively. System performance of a catchment is defined as the ratio of the number of unflooded grid cells to the total number of the grid cells as presented in Eqs. (4)–(6). Flood resilience is an aggregation of system performance during the entire simulation as presented in Eq. (7).

$$g(i,t) = \begin{cases} 1 & d(i,t) \geq h_c \\ 0 & d(i,t) < h_c \end{cases} \quad \text{where } t \in [0, t_n] \tag{4}$$

$$N(t) = \sum_{i=1}^{N} g(i,t) \tag{5}$$

$$p(t) = 1 - \frac{N(t)}{N} \tag{6}$$

$$Res = \frac{1}{t_n} \int_0^{t_n} p(t)dt \tag{7}$$

where $d(i, t)$ is water depth of grid cell i at time t, $g(i, t)$ is the state of grid cell i at time t, h_c is the threshold of flood depth, $N(t)$ is the total number of flooded grid cells, N is the total number of grid cells in a catchment, $p(t)$ is system performance at time t, t_n is the total simulation time, and *Res* is the urban surface flood resilience.

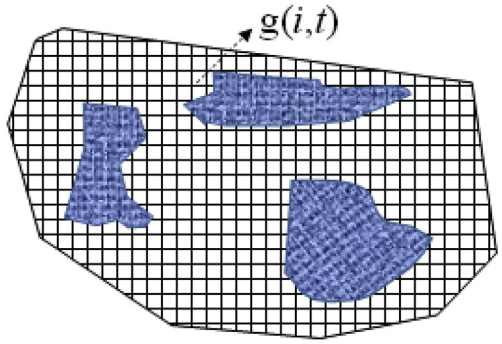

Fig. 2. Schematic of grid cells within or outside the water domain.

2.3. Flood modelling

The Cellular Automata Dual-DraInagE Simulation (CADDIES) model is used for efficient calculation of urban surface flood under a wide range of rainfall storms. It is a novel model based on the principle of cellular automata (CA), which performs a 2D pluvial flood inundation simulation using simple transition rules for modelling complex physical systems (Guidolin et al., 2016). A CA model usually consists of five essential features: a discrete space, the distribution of the neighbor cells, the state of the cells, the discrete time step and the transition rules (Itami, 1994). The first version of CADDIES model CA2D, uses a ranking system instead of directly solving the Manning's equation to evaluate water volume transferred between cells (Ghimire et al., 2013). In this paper, an improved version with a weight-based approach is used as it can achieve faster calculation of transferred water ratios from the central cell to the downstream neighbor cells (intercellular-volume). Furthermore, each grid cell has its own roughness value and infiltration rate to represent soil infiltration and drainage capacity, respectively. The model was demonstrated to have high efficiency and accuracy by various case studies, such as analytical problems, 2D benchmarking test cases for 2D flood modelling proposed by the UK Environment Agency, and real world case studies (Liu et al., 2018; Wang et al., 2018; Webber et al., 2018b). For example, the flood depths from CADDIES and InfoWorks show a satisfactory agreement in a real-world test case in Torquay, UK, and the speed of CADDIES is up to eight times faster than that of InfoWorks (Guidolin et al., 2016). Furthermore, Webber et al. (2018a) demonstrated that CADDIES can identify flood-prone areas and generate flood depths highly correlated (over 97%) with the industry standard approach by Infoworks ICM, using a case study in St Neots of Cambridgeshire, UK.

3. Case study

3.1. Study area

The Siergou area (10.1 km^2) in Dalian, China is used as the case study. The drainage system in this area is of limited capacity and is designed to cope with 1-year return period rainfall only. As shown in Fig. 3(a), the digital elevation data (DEM) of bare terrain has a 5 m × 5 m resolution with the highest and lowest elevations of 223.6 m and −0.6 m, respectively. Urban surface water flows from south Siergou to north Siergou. This area is divided into 31 catchments (in Fig. 4), their boundaries are determined by terrain elevation and their characteristics are shown in Table 1. The sum of grid cells and average values of other parameters of the 31 catchments are presented in the last row ('Total').

As shown in Fig. 3(b), the topography is classified into five different land cover types, i.e. building, green land, manmade surface, road and water, which are assigned with different infiltration rates and roughness parameters in the CADDIES flood model. Different (constant) infiltration rates were applied to different land cover categories to reflect the distinctive urban drainage and soil infiltration capacities (Wang et al., 2018). 82.5% of the Siergou area is developed as buildings and impervious surfaces, while 17.5% of the area remains as permeable green land. According to the drainage capacity of Siergou, the infiltration values of the impervious areas and the green spaces are set to be 30 mm/h and 40 mm/h, respectively.

3.2. Rainfall events

To gain insights into system behaviour under various rainfall intensities, different design rainfall events of 2-h duration of 30-,

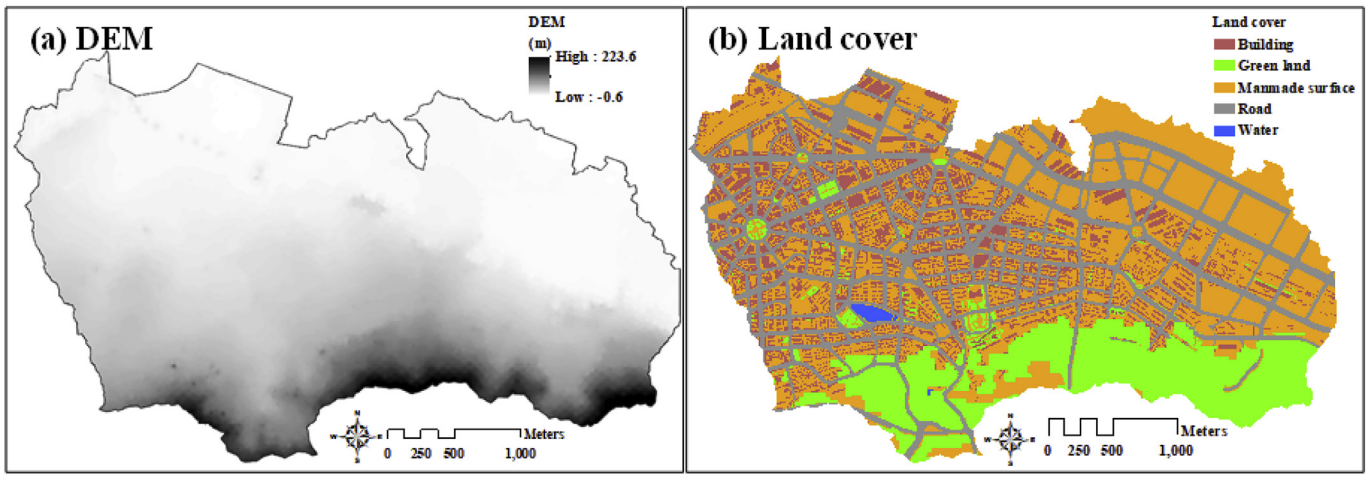

Fig. 3. DEM and land cover data.

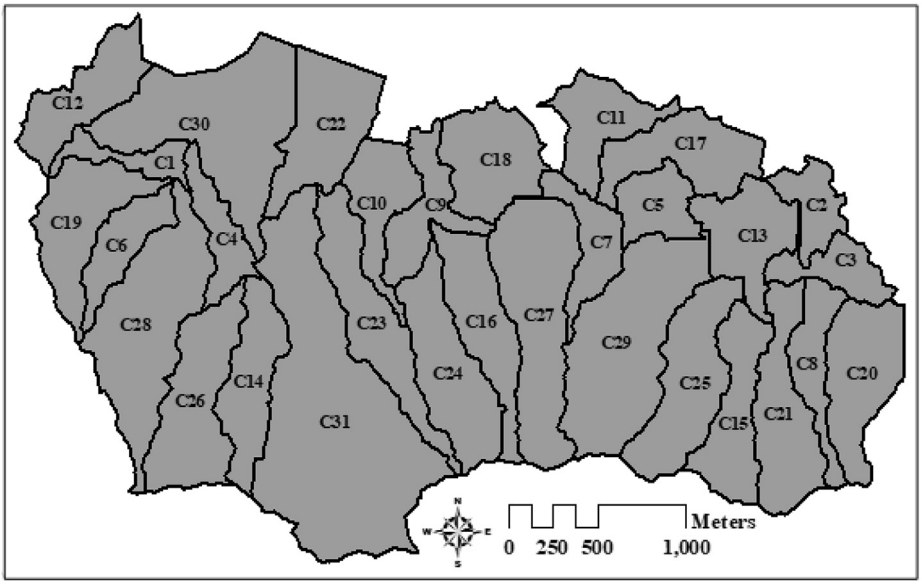

Fig. 4. Distribution of 31 catchments.

50-, 100-, 200-year return periods are generated according to the rainfall intensity equation of Dalian (Zhang et al., 2017), and the rainfall hyetographs are shown in Fig. 5. They have the same location of peak rainfall intensity (r = 0.5).

The rainfall intensity is calculated as

$$i = \frac{1230.157(1 + 0.724\lg P)}{167(t + 5.783)^{0.661}} \quad (8)$$

where i (mm/h) is the average rainfall intensity; P (a) is return period; and t (min) is the duration of rainfall.

4. Results and discussion

4.1. Flood resilience analysis

The maximum flood depth under the 2-h design rainfalls of 30-, 50-, 100- and 200-year return periods are presented in Fig. 6, where color represents the maximum water depth obtained by CADDIES. Fig. 6 shows that extensive flood is observed over the study area, and the flood depth and area increase with the growing rainfall intensity.

The scenario with the 200-year return period rainfall event is chosen to explain the calculation process of urban flood resilience. Fig. 7 presents the temporal evolution of flooded grid cell numbers in the Siergou area, which increases rapidly to a maximum value of 2.1×10^5 at 1.1 h and then decreases mainly due to the drainage of the sewer system. However, it takes about 36 h for the excess runoff to be removed from the Siergou area, due to the limited drainage capacity especially at the downstream catchments.

Water depths at different times are examined to further investigate the dynamics of flooding at each catchment. Flood inundation (depth and area) in Siergou at 2 h, 4 h, 6 h, 8 h, 10 h and 12 h is presented in Fig. 8, where four typical catchments of C2, C5, C30 and C31 are highlighted with colored boundaries. Fig. 8 clearly shows that different catchments have contrasting responses to excess surface water under the 2-h design rainfall of 200-year return period. The flood area of C31 is large at 2 h, but it almost disappears at 4 h. The quick removal of excess surface water can be attributed to the large average slope and green land cover ratio

Table 1
Characteristics of the 31 catchments.

Catchment	Number of grid cells	Land cover ratio (%)					Slope (°)	Length (m)
		Building	Green land	Manmade surface	Road	Water		
C1	4160	18.8	2.1	29.9	49.2	0	0.85	740.3
C2	5414	0	0	86.3	13.7	0	0.56	558.5
C3	5894	0.9	0	72.6	26.5	0	0.58	510.6
C4	5955	21.1	10.5	33.6	34.7	0	1.31	830.2
C5	6370	9.9	0	54.8	35.3	0	0.87	560.0
C6	6745	30.4	7.5	25.4	36.7	0	1.74	980.0
C7	6932	16.8	0.4	60	22.8	0	2.63	1080.1
C8	6961	5.4	26.1	42.6	25.9	0	8.08	1210.6
C9	8217	21.8	0	41	37.2	0	2.08	850.2
C10	8603	29.7	2	37.5	30.8	0	1.57	1080.7
C11	9010	1.2	0	77.4	21.4	0	0.36	990.0
C12	10217	18.5	0	65.4	16.1	0	2.59	980.0
C13	10659	4.6	0	70.1	25.3	0	0.39	740.9
C14	10769	13	22.5	34.1	23	7.4	6.21	1220.4
C15	11038	3.5	53.1	32	11.5	0	10.24	1200.5
C16	11724	23.5	11.3	36.2	29	0	5.32	1410.1
C17	11816	1.5	0	74	24.5	0	0.59	800.6
C18	11868	11.9	0	56.7	31.4	0	1.55	530.5
C19	12557	34.9	0.3	28.8	36.1	0	1.47	1100.9
C20	12978	4.1	31	46.8	18.1	0	8.65	970.4
C21	13273	3.6	55	29.9	11.6	0	12.85	1330.0
C22	13428	22.7	0.3	48.7	28.3	0	1.04	780.7
C23	13730	25	11.7	37.3	25.9	0	3.43	1750.1
C24	14503	16.1	29.8	36.6	17.5	0	8.26	1350.5
C25	14921	10.3	45.7	28.8	15.2	0	9.33	1250.3
C26	15346	20	12	43	25	0	5.88	1310.6
C27	20741	14.6	23.2	37.6	24.6	0	7.3	1560.0
C28	22402	26.4	2.3	36	35.3	0	2.74	1800.5
C29	24896	13.7	32.6	37.3	16.4	0	7.56	1410.3
C30	26054	24.1	0.2	41	34.7	0	1.45	1350.8
C31	47574	10.9	38.7	27.4	22.1	0.9	8.46	2100.0
Total	404755	15.3	17.5	41.9	25.0	0.3	4.93	2897.1

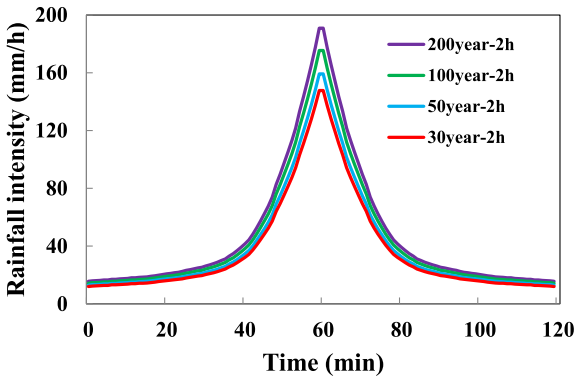

Fig. 5. Design rainfalls of 2-h duration of 30-, 50- 100- and 200-year return periods.

(38.7%) as shown in Table 1. By contrast, C2 suffers from serious flood, with a maximum water depth of 1.3 m and a large flood area of 3.6×10^4 m^2 even at 12 h. The long flood duration in C2 is caused by the insufficient capacity of the local drainage network and the low-lying terrain as shown in Fig. 3(a).

Assuming the flood depth thresholds for building, green land, manmade surface, road and water to be 10 cm, 15 cm, 2 cm, 2 cm and 20 cm, respectively, the number of flooded grid cells in each catchment at different times can be obtained. The results for C2, C5, C30 and C31 under the 2-h design rainfall of 200-year return period are presented in Fig. 9. As shown in Fig. 9(a), the number of flooded grid cells at C30 during the first 45 min of the simulation is low, which then increases rapidly to the peak value at 1.4 h. The numbers of flooded grid cells at 0 h, 1 h, 2 h, 3 h, 6 h, 12 h, 18 h and 24 h are 0, 10389, 11901, 9623, 6017, 4917, 2672 and 0, respectively. The other three catchments show different resilience performance compared to C30. Some catchments can fully recover from the rainfall in a short time while others take longer. For example, C31 has a larger maximum flooded grid cell number of 12069 but it only takes 4 h to recover completely, in comparison to 14413 and 24 h of C30. The full recovery time for C2 is even longer and nearly to 36 h.

The system performance of the four catchments under 2-h design rainfall for 200-year return period are presented in Fig. 9(b). All curves decrease from 1 to a certain level, and then recover to 1. However, the four curves show different characteristics, including the worst system performance and recovery rate. For example, the minimum values of system performance for C2, C5, C30 and C31 are 0.44, 0.60, 0.45 and 0.75, respectively. Even though C31 has a larger maximum flooded grid cell number than C2 and C5, its minimum system performance is better due to the larger total grid cell number.

4.2. Overall flood resilience of 31 catchments

The flood resilience values of the 31 catchments under 2-h design rainfall for 200-year return period are shown in Fig. 10. Results show that catchments located at upstream generally have larger resilience values than those at downstream, e.g. the flood resilience value of C31 is 0.99 compared to 0.69 and 0.65 of C2 and C22, respectively. Nevertheless, urban flood resilience is influenced by a variety of internal/external factors, such as terrain slope, land cover type, drainage capacity, rainfall storm and characteristics of adjacent catchments. For example, despite being located at downstream, C11 has a high resilience value of 0.97 due to its higher average elevation than the adjacent catchment C17.

By the assessment of recovery rate, the proposed resilience

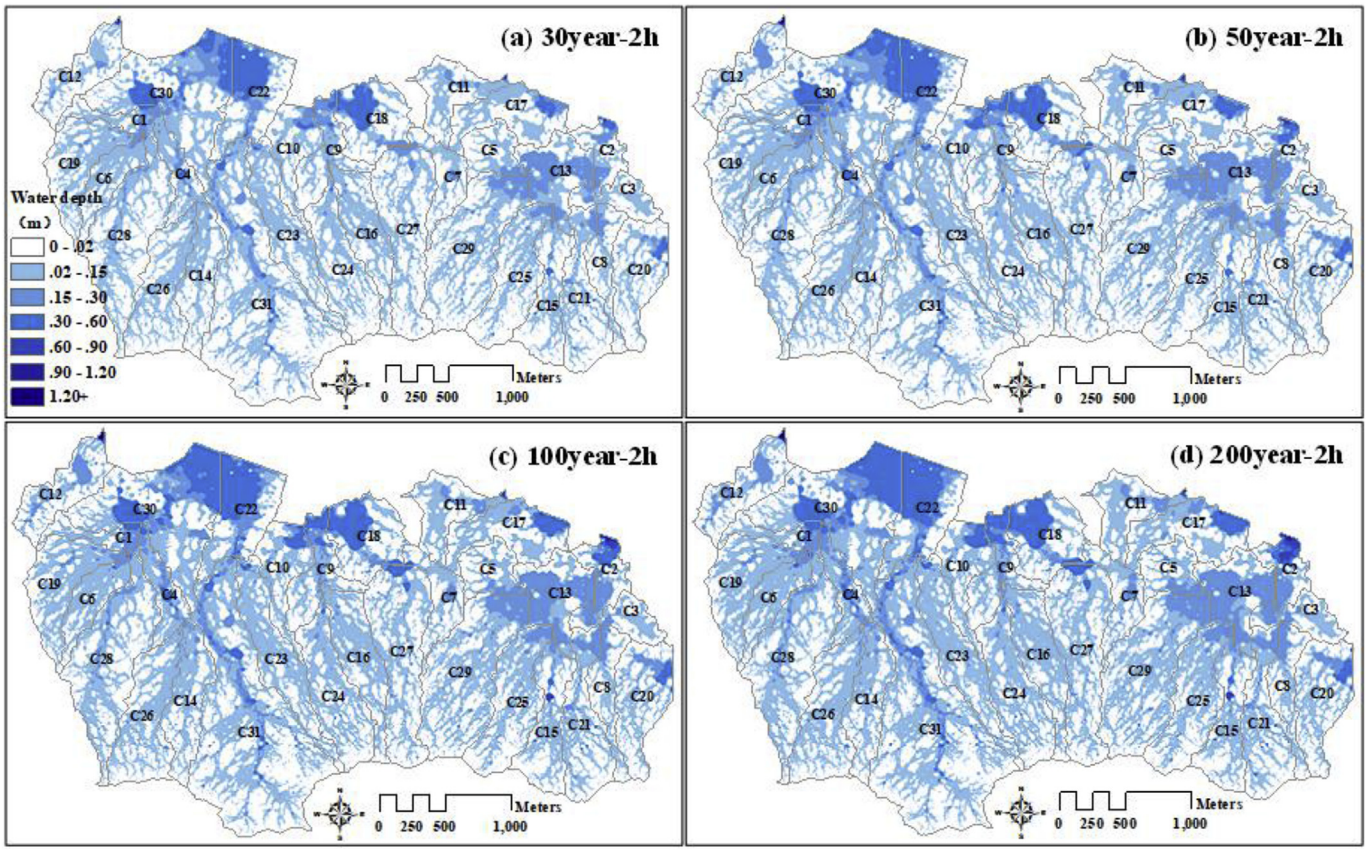

Fig. 6. The maximum flood depths under 2-h design rainfalls of 30, 50, 100, 200-year return periods.

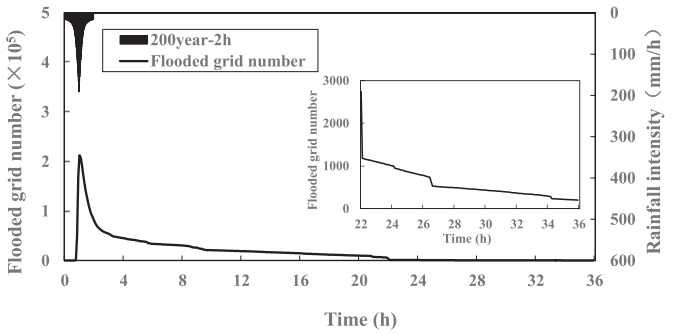

Fig. 7. Flooded grid cell numbers at different times in Siergou under a 2-h design rainfall of 200-year return period.

analysis complements the traditional assessment and provides insights on the real-life consequences of the flood results. For example, Fig. 6(d) shows the maximum water depth of Siergou under the 2-h design rainfall of 200-year return period. The maximum water depths of some grid cells exceed 0.6 m, however, the real-life impacts may not be as serious because the recovery rate is high (e.g. flood resilience value being 0.99).

The flood resilience values of 31 catchments under 2-h design rainfalls of 30-, 50-, and 100-year return periods are shown in Fig. 11. The resilience value generally decreases with the increase in rainfall intensity. Furthermore, results reveal that catchments with low flood resilience are more sensitive to the change in rainfall intensity. For example, the flood resilience values of C2 are 0.86, 0.81, 0.74 and 0.69 under 2-h design rainfalls of 30-, 50-, 100- and 200-year return periods, which are 0.98, 0.98, 0.97 and 0.97 for C1, respectively. A comprehensive resilience assessment of all the catchments reveals the priority areas for interventions to improve flood resilience and reduce flood consequences.

To investigate the influence of the catchment parameters on urban flood resilience, the flood resilience values of the 31 catchments are plotted against average slope, percentage of green land, number of grids and average elevation of catchments in Fig. 12(a)-12(d). As shown in Fig. 12(a), catchments with a large average slope tend to have a large resilience value. For example, the average slope values for C21, C15, C25 and C24 are 12.85, 10.24, 9.33 and 8.26°, respectively, and their flood resilience values are 0.98, 0.99, 0.98 and 0.99, respectively. However, catchments with small average slopes may also have large flood resilience values. For example, the average slopes of C18 and C19 are nearly equal (1.55 and 1.50°), yet there is a big difference in their resilience values (0.77 and 0.99). C19 has a smaller slope but a higher resilience value than C20. This shows that catchment slope is a strong influencing but not the sole factor in determining flood resilience.

Compared to Fig. 12(a), Fig. 12(b) and (c) show a similar relationship between flood resilience and percentage of green land and average elevation, respectively. For example, catchment with a large percentage of green land/elevation (e.g. C15, C25, C31, C24) tends to have a higher resilience value. However, although the percentage of green land of C20 is larger than C19 (i.e., 31% and 0.3%, respectively), C20 has a smaller resilience value than C19 (i.e., 0.94 and 0.99, respectively). This can be explained by other factors, such as characteristics of adjacent catchments or outlet boundary conditions. For example, runoff of C19 mainly flows into the adjacent catchment of C1, while C20 has a closed downstream boundary, thus runoff cannot be drained away quickly.

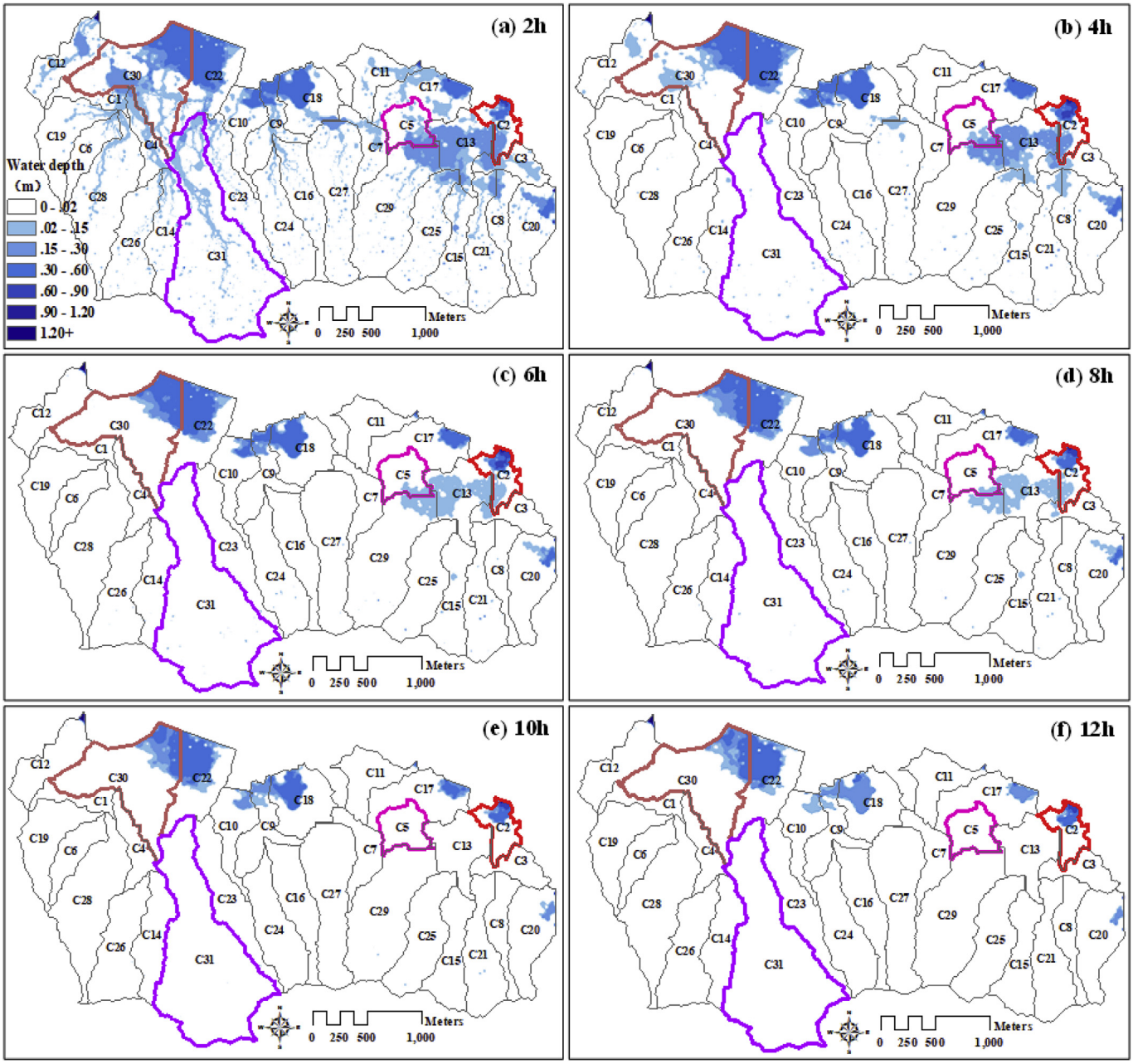

Fig. 8. Water depth at different hours in Siergou under the 2-h design rainfall of 200-year return period.

There is no strong relationship between flood resilience and the number of grids. This is because resilience is calculated as the number of unflooded cells divided by the all grid cells in a catchment, hence catchment size has no impact on the resilience metric value. As urban flood resilience cannot be represented by single factors, the proposed resilience metric provides value for flood management as it can simulate the joint impacts of the relevant factors on flooding resilience.

4.3. Impacts of water depth threshold

The sensitivity of flood resilience to flood depth thresholds is examined by running two scenarios ('HS-2' and 'HS-3') with different threshold values. Their settings are shown in Table 2 in comparison with those used in the previous sections (i.e. 'HS-1'). In 'HS-2', a 10 cm increase is applied for all land cover types compared to 'HS-1'. 'HS-3' uses the same threshold value of 20 cm for every land cover type. The flood resilience values of the 31 catchments at the three scenarios are shown in Fig. 13.

In Fig. 13, the flood resilience values in 'HS-2' are higher than those in 'HS-1'. The flooded grid numbers are lower as the threshold value increases, which leads to improvement in system performance and resilience. However, catchments with smaller resilience values in 'HS-1' tend to have larger increase rates in flood resilience. For example, the flood resilience values of C2, C13 and C22 are 0.69, 0.83 and 0.65 in 'HS-1', which increase to 0.78, 0.92 and 0.73 in 'HS-2'. The increase rate of flood resilience of C2, C13 and C22 are 13%, 11% and 12%, respectively. On the contrary, the flood resilience values of C23, C24 and C25 in 'HS-2' all increase by 1% only. Although flood depth thresholds for green land and water

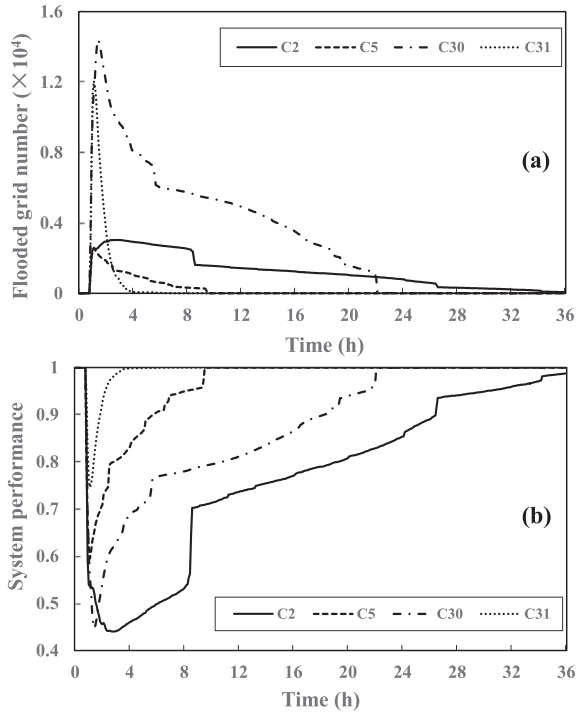

Fig. 9. Flooded grid cell numbers and system performance at different times for four catchments under 2-h design rainfall of 200-year return period.

in 'HS-3' are smaller than those in 'HS-2', the resilience values are generally larger in 'HS-3'. This shows that the threshold values for impervious surfaces have a larger impact on the resilience results.

4.4. Comparison of metrics

The urban flood resilience metric proposed in this study (*Res* by Eq. (7)) is compared with the metric reported in Mugume et al. (2015) (Res_0 by Eq. (3)). The comparison of resilience values for 31 catchments under four 2-h design rainfall events of 30-, 50-, 100-, 200-year return periods are shown in Fig. 14.

It can be seen that similar results (strong positive correlation) are obtained for the 31 catchments under the four design rainfall events of 30-, 50-, 100-, 200-year return periods. Both Res_0 and *Res* tend to reduce with the increase in rainfall intensity. Catchments with smaller resilience values can be identified as vulnerable areas. The values of Res_0 are negative for some catchments, e.g. −1.08, −0.89, −0.38 and −0.32 for C22, C2, C18 and C30, respectively. The negative value indicates that the corresponding catchment receives urban runoff from its adjacent catchments which results in a larger total flood volume. For these catchments, adaptation strategies need to be applied in their adjacent catchments to alleviate flooding.

Nevertheless, the relative resilience values for two catchments measured by Res_0 can be very different from those by *Res*. As shown in Fig. 14 (d), the values of *Res* for C13 and C30 are nearly equal (i.e., 0.82), but there is a big difference in the values of Res_0 (i.e., 0.50 and −0.32). A similar pattern is observed between C18 and C30. This can be explained by the detailed resilience performance of the catchments under 2-h design rainfall for 200-year return period shown in Fig. 15. It can be seen that the system performance curves for C13 and C30 are very different in terms of failure magnitude, failure duration and recovery rate (Meng et al., 2018). The worst system performance for C13 and C30 are 0.28 and 0.45 and their time for full recovery are 9.3 h and 22.0 h, respectively. However, their flood severity values are equal hence their *Res* values are the same. This shows that some details are lost when simplifying the system failure and recovery curve as a rectangular.

4.5. Effects of adaptation strategies

4.5.1. Adaptation scenarios design

Adaptation strategies, such as conventional piped solutions, sustainable drainage system (SuDS) (e.g. green roofs, rainwater harvesting and attenuation tanks, infiltration trenches, permeable pavement), green infrastructure, are widely adopted to manage

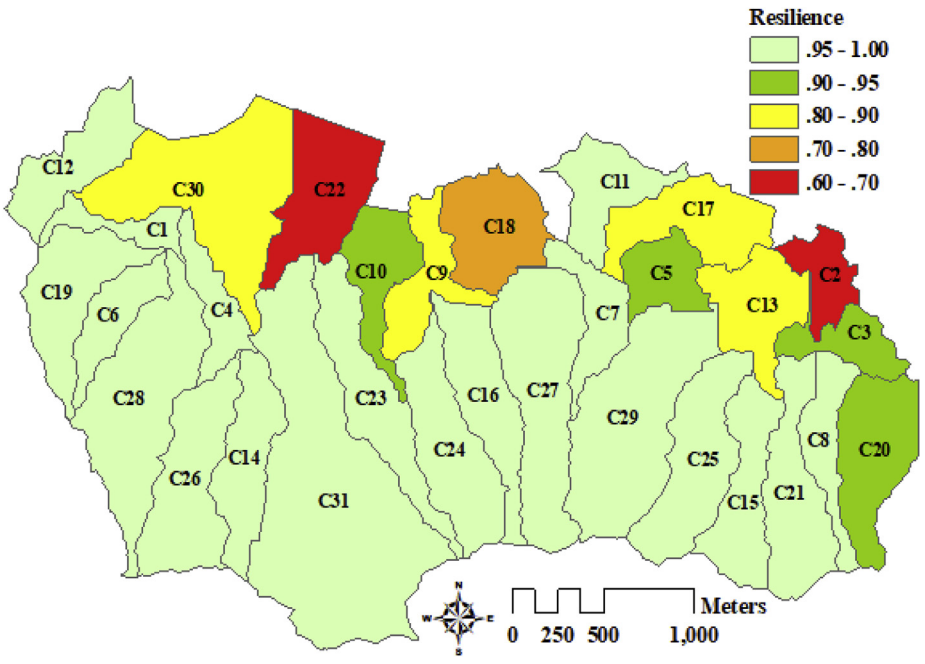

Fig. 10. Flood resilience of 31 catchments under 2-h design rainfall for 200-year return period.

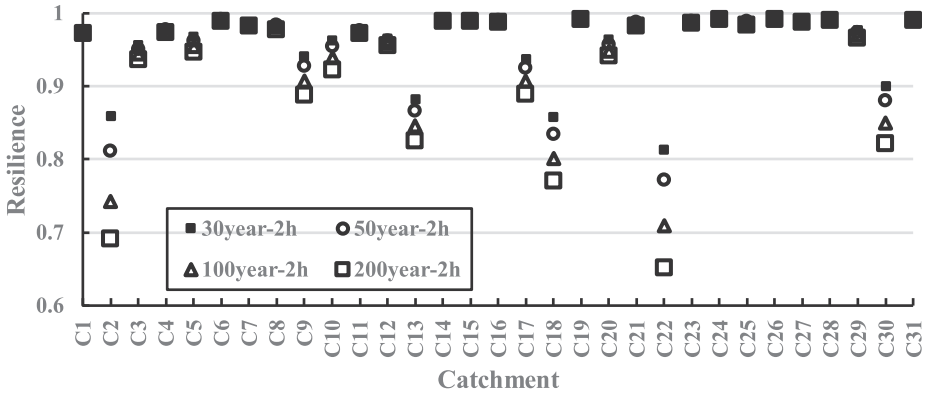

Fig. 11. Flood resilience of 31 catchments under 2-h design rainfalls for 30-, 50-, 100- and 200-year return periods.

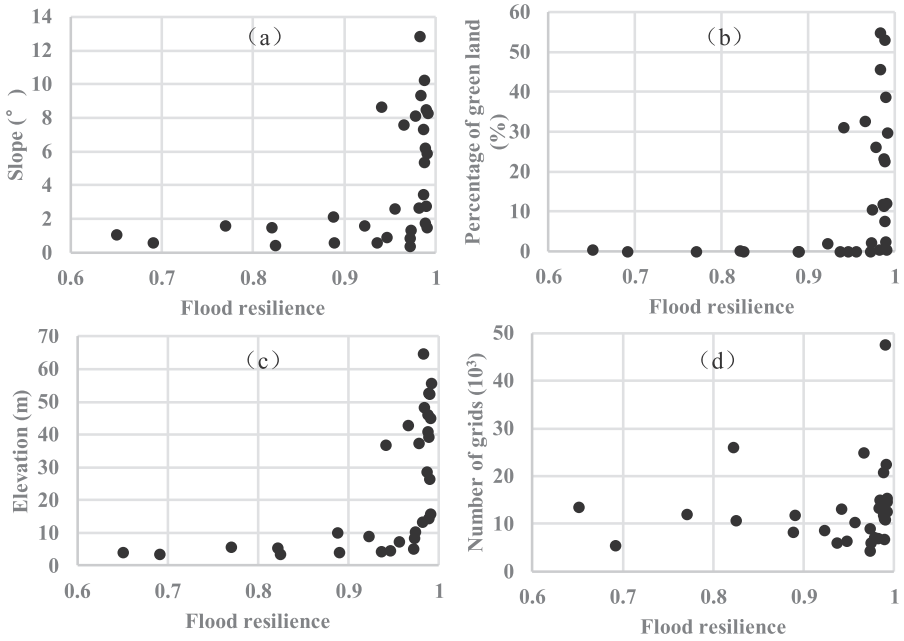

Fig. 12. The relationship between flood resilience values of 31 catchments under 2-h design rainfall of 200-year return period and the corresponding catchment parameters of average slope, percentage of green land, number of grids and average elevation of catchments.

Table 2
Scenarios with different thresholds of water depth (unit: cm).

Scenario	Land cover				
	Building	Green land	Manmade surface	Road	Water
HS-1	10	15	2	2	20
HS-2	20	25	12	12	30
HS-3	20	20	20	20	20

flood risk by slowing down and reducing the quantity of urban surface water runoff. The adoption of these adaptation strategies for improving urban surface flood resilience is consistent with the ultimate goal of Sponge city construction in China. The combinational use of different adaptation strategies is found to be effective in improving system resilience (Sweetapple et al., 2018). Hence, the selection of intervention measures at different locations in a catchment is needed. Though there are limitations in using 2D urban surface flood modelling for assessing intervention options, satisfactory representations can be made by adjustment of the parameters that control flow input, output and transmission speed in each cell (Webber et al., 2018b). In this paper, adjustment of infiltration rate is used to represent the application of various intervention options. Three adaptation strategies were modelled and tested, i.e., adaptation measures only adopted in the downstream catchment (DS), adaptation measures only adopted in the upstream catchment (US) and adaptation measures both adopted in the upstream and downstream catchments (UDS).

C2, C13, C22 and C30 are chosen for analysing the effectiveness of the adaptation strategies as they have relatively smaller resilience values. The four catchments are classified into two vulnerable areas of I (i.e., C2 and C13) and II (i.e., C22 and C30) as highlighted in Fig. 16. According to the direction of runoff flow through catchments, the downstream catchments in areas I and II are C2 and C22, respectively. The grid cells with larger maximum flood water depth were preferentially chosen for adaptation. As seen in Table 3, the total numbers of grid cells with adaptation measures for area I and II are 2409 and 6582, respectively and their layouts are shown in Fig. 16. Note that the same number of grid cells is intervened under

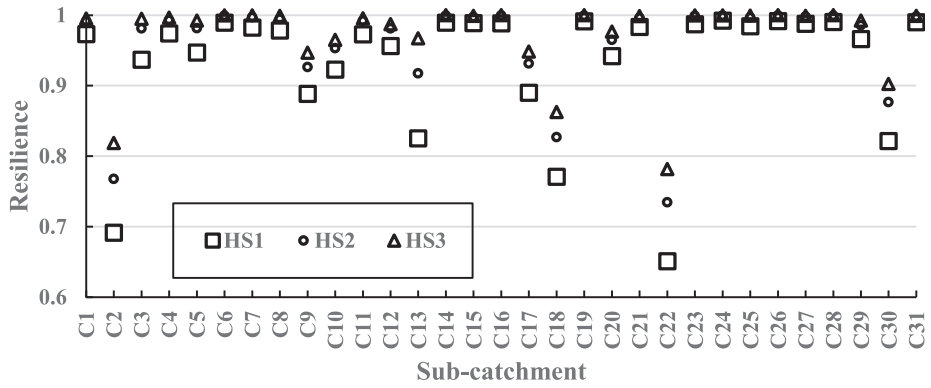

Fig. 13. Flood resilience of the 31 catchments under three scenarios with different flood depth thresholds.

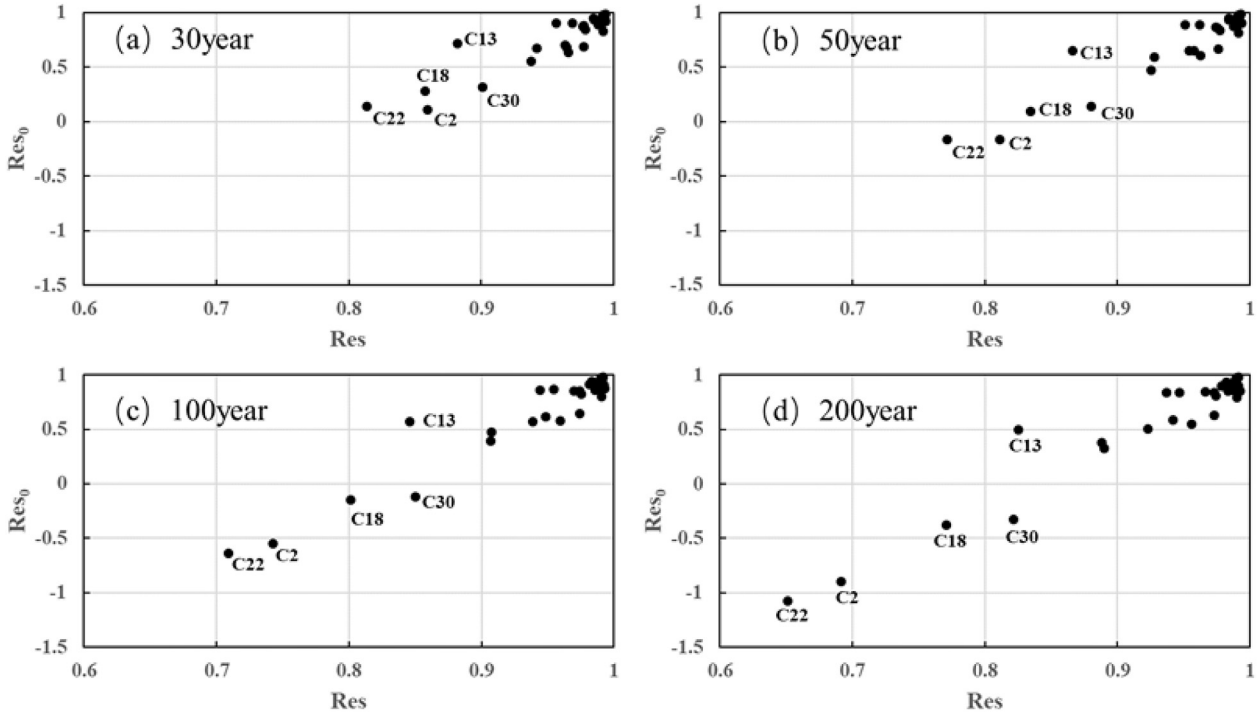

Fig. 14. Comparison between the values of Res_0 and *Res* under 2-h design rainfall events of 30, 50, 100 and 200-year return periods.

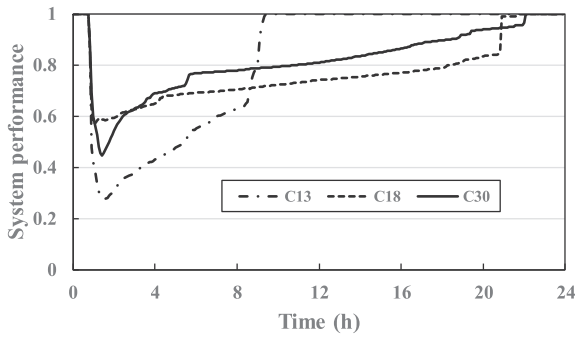

Fig. 15. System performance at different times for three catchments under 2-h design rainfall event of 200-year return period.

the three scenarios in an area; further, the adaptation measures adopted are not specific interventions but rather combinations of various intervention options. The infiltration rate for the grid cells with adaptation measures adopted is assumed to be 60 mm/h to reflect the effects of capturing, storing of rainfall and infiltrating water.

4.5.2. Effect of adaptation strategies on urban surface flood resilience

The 2-h design rainfall of 200-year return period is used to further investigate the effects of adaptation strategies on the improvement of urban surface flood resilience. The flood resilience values of *Res* for catchments of C2, C13, C22 and C30 under the adaptation scenarios of S, DS, US and UDS are shown in Fig. 17. It can be seen that resilience values increase for all the four catchments under the scenarios of DS, US and UDS compared to the 'do nothing' scenario ('S').

In Fig. 17, adaptation strategies help enhance flood resilience by increasing the drainage capacity. However, the responses to the adaptation scenarios of DS, US and UDS for each catchment are different. For example, the resilience values of C2 under S, DS, US

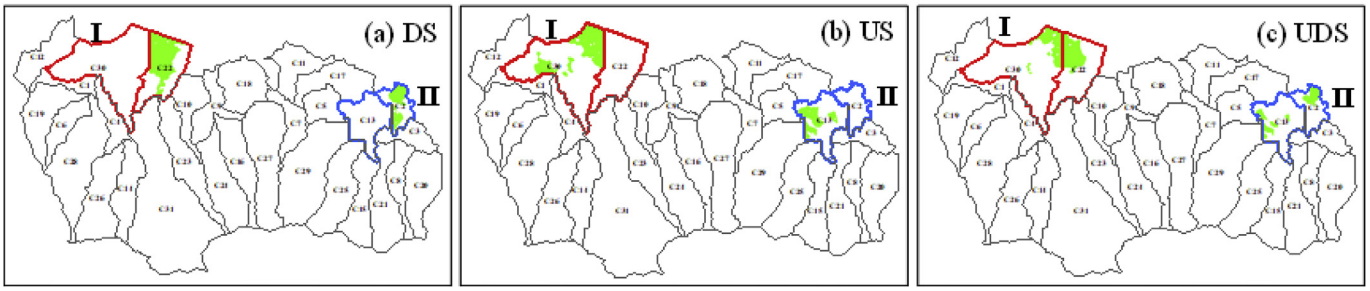

Fig. 16. Layouts of adaptation measures. (a) For downstream catchments of C2 and C22, (b) for upstream catchments of C13 and C30, and (c) for the downstream and upstream catchments of C2, C13, C22, C30.

Table 3
Adaptation scenarios and corresponding parameters values.

Adaptation Scenario		Catchment	Number of grid cells adopted adaptation measures	Infiltration (mm/h)
DS	DS I	C2	2409	60
	DS II	C22	6582	60
US	US I	C13	2409	60
	US II	C30	6582	60
UDS	UDS I	C2	1204	60
		C13	1205	60
	UDS II	C22	3291	60
		C30	3291	60

and UDS are 0.69, 0.81, 0.71 and 0.79, respectively. The increase rate of resilience under DS, US and UDS are 17.6%, 3.0% and 14.6% compared to the 'do nothing' scenario S. Therefore, scenario DS shows the greatest improvement in urban surface flood resilience for C2. Similarly, C13 (located at upstream) could achieve the largest resilience increase in the US scenario. This demonstrates that the best effects of adaptation strategies for each catchment in area I will occur only when the adaptation measures are adopted within their own catchments. However, in terms of the overall resilience improvement in the entire area I, the DS scenario can achieve almost the same effects as the UDS scenarios. This shows that most runoff in area I is generated in the downstream catchment DS, so it is not effective to reduce runoff generation from upstream catchments.

Nevertheless, the resilience values of C22 and C30 show different characteristics compared to those of C2 and C13 shown in Fig. 17. For example, the resilience values of C22 under S, DS, US and UDS are 0.65, 0.77, 0.74 and 0.78, respectively, and the corresponding values for C30 are 0.82, 0.86, 0.87 and 0.88, respectively. Therefore, adaptation measures adopted in the upstream and downstream catchments (UDS) can achieve the best effects in enhancing resilience of each catchment in area II. This implies that reducing the runoff generation from the entire area including the upstream catchment is significant for area II.

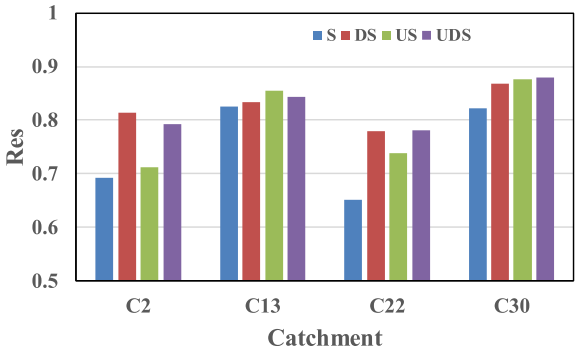

Fig. 17. Resilience values of Res for catchments of C2, C13, C22 and C30 under the 2-h design rainfall event of 200-year return period.

In summary, the resilience assessment using the proposed resilience metric can identify the effective adaptation strategy for an area covering more than one urban drainage catchment. It is impossible to apply a universal adaptation strategy for different areas, due to different catchment characteristics and mechanisms that cause flooding. Hence, resilience analysis should be performed for flood intervention planning and design in the sponge city development process.

5. Conclusions

In this paper a new grid cell based metric is proposed to assess flood resilience for urban surface flood management. A CA-based urban two-dimensional model is used to simulate surface flooding. Flood resilience values of different catchments are compared and analyzed using a case study of the Siergou in Dalian, China. The effectiveness of adaptation strategies in enhancing urban surface flood resilience is investigated. The following conclusions are drawn:

1) The grid cell based metric can accurately reveal the flooding dynamics of urban drainage catchments in response to extreme events, i.e., the varying number of flooded grid cells at a high resolution such as 5 m × 5 m in the case study. Flood resilience is influenced by the joint impact of different urban drainage catchment characteristics such as different land cover percentages, catchment average slope and drainage capacity. The coupling of 2-D modelling and grid-cell based metric enables comprehensive resilience assessment of all catchments. It reveals the priority areas for flood interventions and provides useful evidence for informed decision making towards large-scale investments in urban flood management.
2) Though similarities exist between the two resilience values of the grid cell based and the simplified metrics in most urban

drainage catchments, there is a striking difference between the values by the two metrics in some catchments. The difference is caused by the simplification of the system performance curve in the simplified metric, resulting in an inaccurate representation of failure magnitude, failure duration and recovery rate. Nevertheless, it is found that the simplified metric can have a negative value in a catchment due to a large volume of urban runoff from adjacent catchments, which is useful in identifying the source of runoff and thus effective intervention strategies.

3) Comparing different flood adaptation strategies shows that reducing the runoff generation from the upstream catchment alone is not effective in flood resilience improvement. Instead, both upstream and downstream catchments should be considered together to develop the most effective measures for resilience enhancement in the whole area. This implies that resilience assessment using the new metric is critical to develop effective adaptation strategies for urban catchments of different characteristics in the sponge city development process.

Impacts of terrain features on urban flood resilience should be further explored with a flood model in future study, which can accurately represent hydrological processes in urban areas and flow dynamics in drainage networks. Further, there is a need to evaluate the influence on the resilience results from the simplified simulation of drainage by sewer networks in CADDIES model using the constant infiltration approach.

Acknowledgments

This research was funded by the UK Engineering and Physical Sciences Research Council under the Building Resilience into Risk Management project (EP/N010329/1). The first author was funded by the China Scholarship Council.

References

Batica, J., 2015. Methodology for Flood Resilience Assessment in Urban Environments and Mitigation Strategy Development. University of Nice - Sophia Antipolis, France.
Bertilsson, L., Wiklund, K., de Moura Tebaldi, I., Rezende, O.M., Veról, A.P., Miguez, M.G., 2019. Urban flood resilience — a multi-criteria index to integrate flood resilience into urban planning. J. Hydrol. 573, 970–982.
Bocchini, P., Frangopol, D.M., Ummenhofer, T., Zinke, T., 2013. Resilience and sustainability of civil infrastructure: toward a unified approach. J. Infrastruct. Syst. 20 (2), 04014004.
Bruneau, M., Chang, S.E., Eguchi, R.T., Lee, G.C., O'Rourke, T.D., Reinhorn, A.M., Shinozuka, M., Tierney, K., Wallace, W.A., Von Winterfeldt, D., 2003. A framework to quantitatively assess and enhance the seismic resilience of communities. Earthq. Spectra 19 (4), 733–752.
Butler, D., Farmani, R., Fu, G., Ward, S., Diao, K., Astaraie-Imani, M., 2014. A new approach to urban water management: safe and sure. Procedia Eng. 89, 347–354.
Chen, A.S., Evans, B., Djordjević, S., Savić, D.A., 2012. A coarse-grid approach to representing building blockage effects in 2D urban flood modelling. J. Hydrol. 426, 1–16.
Chen, K.-F., Leandro, J., 2019. A conceptual time-varying flood resilience index for urban areas: munich city. Water 11 (4), 830.
Defra, 2016. Creating a Great Place for Living Enabling Resilience in the Water Sector, UK.
Gallego-Lopez, C., Essex, J., 2016. Designing for Infrastructure Resilience, UK.
Ganin, A.A., Massaro, E., Gutfraind, A., Steen, N., Keisler, J.M., Kott, A., Mangoubi, R., Linkov, I., 2016. Operational resilience: concepts, design and analysis. Sci. Rep. 6, 19540.
Ghimire, B., Chen, A.S., Guidolin, M., Keedwell, E.C., Djordjević, S., Savić, D.A., 2013. Formulation of a fast 2D urban pluvial flood model using a cellular automata approach. J. Hydroinf. 15 (3), 676–686.
Guidolin, M., Chen, A.S., Ghimire, B., Keedwell, E.C., Djordjević, S., Savić, D.A., 2016. A weighted cellular automata 2D inundation model for rapid flood analysis. Environ. Model. Softw 84, 378–394.
Guidolin, M., Duncan, A., Ghimire, B., Gibson, M., Keedwell, E., Chen, A.S., Djordjevic, S., Savic, D., 2012. CADDIES: A New Framework for Rapid Development of Parallel Cellular Automata Algorithms for Flood Simulation, Hamburg, Germany.
Hammond, M.J., Chen, A.S., Djordjević, S., Butler, D., Mark, O., 2015. Urban flood impact assessment: a state-of-the-art review. Urban Water J. 12 (1), 14–29.
Hirabayashi, Y., Mahendran, R., Koirala, S., Konoshima, L., Yamazaki, D., Watanabe, S., Kim, H., Kanae, S., 2013. Global flood risk under climate change. Nat. Clim. Change 3 (9), 816–821.
Holling, C.S., 1973. Resilience and stability of ecological systems. Annu. Rev. Ecol. Systemat. 4 (1), 1–23.
Holling, C.S., 1996. Engineering Resilience versus Ecological Resilience, USA.
Hu, M., Zhang, J., Huang, J., 2018. Assessing social-ecological system resilience in mainland China. Pol. J. Environ. Stud. 27 (3), 1085–1096.
Hwang, H., Lansey, K., Quintanar, D.R., 2015. Resilience-based failure mode effects and criticality analysis for regional water supply system. J. Hydroinf. 17 (2), 193–210.
Itami, R.M., 1994. Simulating spatial dynamics: cellular automata theory. Landsc. Urban Plan. 30 (1–2), 27–47.
Jenkins, K., Surminski, S., Hall, J., Crick, F., 2017. Assessing surface water flood risk and management strategies under future climate change: insights from an agent-based model. Sci. Total Environ. 595, 159–168 (2017).
Jia, H., Wang, Z., Zhen, X., Clar, M., Shaw, L.Y., 2017. China's sponge city construction: a discussion on technical approaches. Front. Environ. Sci. Eng. 11 (4), 18.
Juan-García, P., Butler, D., Comas, J., Darch, G., Sweetapple, C., Thornton, A., Corominas, L., 2017. Resilience theory incorporated into urban wastewater systems management. State of the art. Water Res. 115, 149–161.
Kotzee, I., Reyers, B., 2016. Piloting a social-ecological index for measuring flood resilience: a composite index approach. Ecol. Indicat. 60, 45–53.
Löwe, R., Urich, C., Domingo, N.S., Mark, O., Deletic, A., Arnbjerg-Nielsen, K., 2017. Assessment of urban pluvial flood risk and efficiency of adaptation options through simulations–A new generation of urban planning tools. J. Hydrol. 550, 355–367 (2017).
Lee, E., Kim, J., 2017a. Convertible operation techniques for pump stations sharing centralized reservoirs for improving resilience in urban drainage systems. Water 9 (11), 843.
Lee, E.H., Kim, J.H., 2017b. Development of resilience index based on flooding damage in urban areas. Water 9 (6), 428.
Liao, K.-H., 2012. A theory on urban resilience to floods—a basis for alternative planning practices. Ecol. Soc. 17 (4), 48.
Linkov, I., Bridges, T., Creutzig, F., Decker, J., Fox-Lent, C., Kröger, W., Lambert, J.H., Levermann, A., Montreuil, B., Nathwani, J., 2014. Changing the resilience paradigm. Nat. Clim. Change 4 (6), 407.
Liu, H., Wang, Y., Zhang, C., Chen, A.S., Fu, G., 2018. Assessing real options in urban surface water flood risk management under climate change. Nat. Hazards 94 (1), 1–18.
Meng, F., Fu, G., Farmani, R., Sweetapple, C., Butler, D., 2018. Topological attributes of network resilience: a study in water distribution systems. Water Res. 143, 376–386.
Miguez, M.G., Veról, A.P., 2017. A catchment scale Integrated Flood Resilience Index to support decision making in urban flood control design. Environ. Plan. B 44 (5), 925–946.
Morrison, A., Westbrook, C.J., Noble, B.F., 2017. A review of the flood risk management governance and resilience literature. J. Flood Risk Manag. 11 (3), 291–304.
Mugume, S.N., Gomez, D.E., Fu, G., Farmani, R., Butler, D., 2015. A global analysis approach for investigating structural resilience in urban drainage systems. Water Res. 81, 15–26.
Ofwat, 2017. Delivering Water 2020: Our Final Methodology for the 2019 Price Review, UK.
Pitt, M., 2008. Learning Lessons from the 2007 Floods, UK.
Restemeyer, B., Woltjer, J., van den Brink, M., 2015. A strategy-based framework for assessing the flood resilience of cities–A Hamburg case study. Plann. Theor. 16 (1), 45–62.
Simonovic, S., 2016. From risk management to quantitative disaster resilience–a paradigm shift. Int. J. Saf. Secur. Eng. 6 (2), 85–95.
Sweetapple, C., Fu, G., Farmani, R., Meng, F., Ward, S., Butler, D., 2018. Attribute-based intervention development for increasing resilience of urban drainage systems. Water Sci. Technol. 77 (6), 1757–1764.
Wang, Y., Chen, A.S., Fu, G., Djordjević, S., Zhang, C., Savić, D.A., 2018. An integrated framework for high-resolution urban flood modelling considering multiple information sources and urban features. Environ. Model. Softw 107, 85–95.
Webber, J., Booth, G., Gunasekara, R., Fu, G., Butler, D., 2018a. Validating a rapid assessment framework for screening surface water flood risk. Water Environ. J. 1–16.
Webber, J., Gibson, M., Chen, A., Savic, D., Fu, G., Butler, D., 2018b. Rapid assessment of surface-water flood-management options in urban catchments. Urban Water J. 1–8.
Yin, J., Yu, D., Wilby, R., 2016. Modelling the impact of land subsidence on urban pluvial flooding: a case study of downtown Shanghai, China. Sci. Total Environ. 544, 744–753.
Zhang, C., Wang, Y., Li, Y., Ding, W., 2017. Vulnerability analysis of urban drainage systems: tree vs. Loop networks. Sustainability 9 (3), 397.